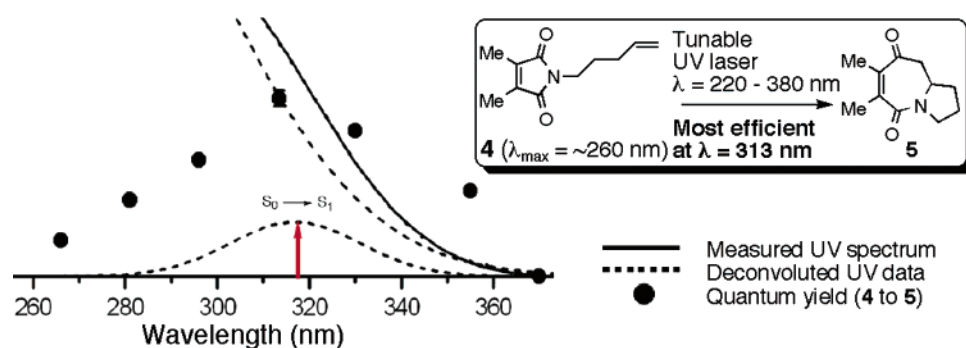


## Reaction Optimization and Mechanism in Maleimide [5 + 2] Photocycloaddition: A Dual Approach Using Tunable UV Lasers and Time-Dependent DFT

David M. E. Davies,<sup>†</sup> Craig Murray,<sup>‡</sup> Malcolm Berry,<sup>¶</sup> Andrew J. Orr-Ewing,<sup>\*,†</sup> and Kevin I. Booker-Milburn<sup>\*,†</sup>

*School of Chemistry, University of Bristol, Cantock's Close, Bristol, United Kingdom, BS8 1TS,  
Department of Chemistry, University of Pennsylvania, 231 South 34th Street, Philadelphia,  
Pennsylvania 19104, and Continuous Chemistry, Strategic Technologies, Medicines Research Centre,  
GlaxoSmithKline, Stevenage, United Kingdom, SG1 2NY*

Received November 9, 2006



An in-depth study of the intramolecular [5 + 2] photocycloaddition of maleimides using tunable UV lasers has demonstrated that the peak in quantum yield and rate both occur at wavelengths some 50 nm red shifted from the maxima observed in the UV spectra. A detailed explanation for these findings using time-dependent DFT calculations is presented, and the implications for a previously adopted mechanism are discussed.

### Introduction

Preparative organic photochemistry is a powerful technique for the modern synthetic chemist, as it offers a clean and often unique approach to complex molecular architectures and can be used as an alternative technique for various chemical transformations used in research. For many years, chemists have relied on low- and medium-pressure mercury light sources to perform photochemistry in an immersion well or Rayonet-style apparatus. Although medium-pressure mercury lamps are extensively used in research, they are broadband emitters, and irradiation can lead to unwanted secondary photoproducts and photopolymerization, resulting in difficult purification steps. Furthermore, the more intense emission wavelengths of a mercury lamp may not match the absorption features of the target chromophore, leading to inefficient irradiation of the target substrate. Some of these undesirable features can be attenuated

but not eliminated in all cases using various glassware or solution-based filters.

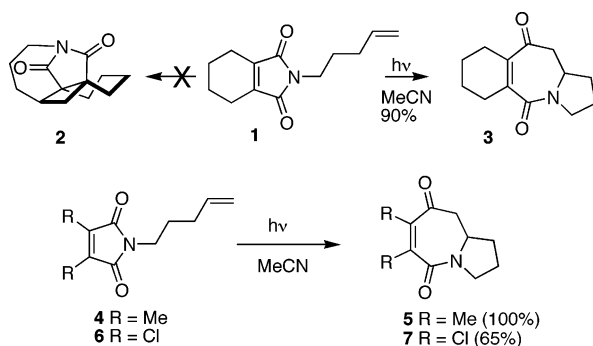
Recently, we established a tunable visible and ultraviolet laser facility for organic photochemistry. The lasers at our disposal provide monochromatic radiation over the majority of the visible and UV region (220–800 nm) and allow for irradiation of substrates at precisely selected wavelengths such as where absorption is maximized. The laser facility is also advantageous in that careful choice of irradiation wavelength can, in principle, avoid the formation of secondary photoproducts. The high (and precisely determined) incidental powers allow the investigation of reactions on the 1–10 mmol scale. This facility is envisaged to be particularly useful for the investigation of wavelength-dependent kinetics and quantum yields<sup>1</sup> of a range of photochemical reactions with exquisite levels of precision simply not possible with conventional UV sources. The invaluable mechanistic information that will arise from these studies will then be fed into various other current research programs such as the design of new photochemical reactions and flow reactors.<sup>2</sup>

<sup>†</sup> University of Bristol.

<sup>‡</sup> University of Pennsylvania.

<sup>¶</sup> GlaxoSmithKline.

## SCHEME 1. [5 + 2] Photocycloaddition of Maleimides



A reaction of ongoing interest has been the [5 + 2] cycloaddition of maleimides which was previously observed by us while investigating the photocycloaddition of tetrahydrophthalimide **1**.<sup>3</sup> Instead of the expected [2 + 2] product **2**, the tricyclic azepine **3** was formed exclusively (Scheme 1). The reaction was found to be general for a wide range of maleimides and is currently being used by us as the key step in the total synthesis of perhydroazazulene-containing natural products such as those of the *Stemona* alkaloids family.<sup>4</sup> For example, irradiation of *N*-pentenyl-2,3-dimethyl- (**4**) and *N*-pentenyl-2,3-dichloromaleimide (**6**) using medium-pressure mercury lamps (in pyrex) gives the [5 + 2] cycloaddition products **5** and **7**, respectively (Scheme 1).

These reactions showed significant similarities to previous detailed work carried out by Mazzocchi et al. on the inter- and intramolecular cycloadditions of *N*-substituted phthalimides with alkenes.<sup>5</sup> These detailed studies led this group to propose two plausible mechanisms for the photocycloaddition of phthalimides, one of which we have generally adopted to explain our results with maleimides (Scheme 2). The first involves a concerted pathway where it is convenient to propose direct [2 + 2] cycloaddition of the pentenyl alkene and the amide  $\pi$ -system represented by the resonance form **8b** to form the zwitterionic species **9**, which then undergoes an ionic fragmentation of the C–N bond to form the [5 + 2] photoproduct **10**. The second is a stepwise radical mechanism, where, upon irradiation, the excited state **11** undergoes cyclization to **12** followed by ring closure to **9**, which then undergoes spontaneous C–N bond cleavage to **10**, as before.

In the case of phthalimides, the first mechanism was favored by Mazzocchi et al.<sup>5</sup> because detailed studies demonstrated that both *cis*- and *trans*-2-butene underwent stereospecific intermolecular cycloaddition with *N*-methyl phthalimide, thus retaining the alkene geometry in the [5 + 2] products. However, the

second mechanism cannot be ruled out, as the resulting biradical intermediate **12** may close at a faster rate than bond rotation, which would also result in retention of the original alkene geometry (Note: for the purpose of clarity, all mechanisms depicted in Scheme 2 show retention of stereochemistry in the formation of **10**). Mazzocchi et al. concluded that both of these mechanisms were likely to be fast, singlet manifold processes, as triplet quenching did not retard the reactions; on the contrary, phthalimide itself was shown to undergo efficient intermolecular [5 + 2] cycloaddition with dienes.

Mazzocchi also considered<sup>5d</sup> alternative PET mechanisms for the cycloaddition of phthalimides. Both Griesbeck and Mariano have worked extensively on the synthetic and mechanistic aspects of phthalimide PET chemistry, and there is now a wealth of mechanistic detail known about these processes.<sup>6</sup> Although Mazzocchi found that products could be isolated from irradiation of phthalimide with appropriate alkenes by interception of reactive PET intermediates with alcohols, this mechanism was discounted for the inter- and intramolecular [5 + 2] cycloaddition sequence. In particular, intermolecular cycloadditions with substituted alkenes gave the “wrong” regiochemistry to be consistent with a PET pathway.

For maleimides, we have also considered a further possible stepwise mechanism involving the singlet ( $S_1$ ) excited state (**13**) resulting from initial carbonyl  $n \rightarrow \pi^*$  excitation. Mechanism **3** would proceed from  $\alpha$ -cleavage of the C–N acyl bond in **13** leading to the diradical **14** which undergoes synchronous [5 + 2] cyclization to **10**. Mazzocchi et al. disfavored this type of mechanism because irradiation of the parent phthalimide in the absence of an alkene gave no expected products resulting from such a cleavage process. However, it should be noted that such  $\alpha$ -cleavage reactions of acyclic imides are documented,<sup>7</sup> and we suggest this mechanism cannot be ruled out for maleimides on the basis of a negative result from a comparable but different phthalimide chromophore. For example, although photochemical cleavage of the C–C(O) bond in succinimides is well documented,<sup>8</sup> there is also strong precedent from the work of Fischer<sup>9</sup> and De Schryver<sup>10</sup> that azetidino-2,4-diones undergo N–C(O) cleavage and further reaction via a biradical sequence. *N*-Phenyl imides have been known for some time to undergo preparatively useful photochemical ring enlargements via a singlet N–C(O) cleavage/recombination sequence.<sup>11</sup> Both N–C(O) and C–C(O) reactions of *N*-methylpyrrolidone have been reported by Mazzocchi.<sup>12</sup> In the case of maleimide, it could be rationalized that C–C(O) cleavage is unlikely, as it would result in the formation of a localized high-energy vinyl radical rather than the delocalized amide radical (in **14**) resulting from the alternative N–C(O) cleavage of **13**.

(1) For examples of wavelength dependence in organic and organometallic chemistry, see: (a) Dauben, W. G.; Disanayaka, B.; Funhoff, D. J. H.; Kohler, B. E.; Schilke, D. E.; Zhou, B. *J. Am. Chem. Soc.* **1991**, *113*, 8367. (b) Dauben, W. G.; Zhou, B.; Lam, J. Y. L. *J. Org. Chem.* **1997**, *62*, 9005. (c) Jakúbek, V.; Lees, A. J. *Inorg. Chem.* **2000**, *39*, 5779.

(2) Hook, B. D. A.; Dohle, W.; Hirst, P. R.; Pickworth, M.; Berry, M. B.; Booker-Milburn, K. I. *J. Org. Chem.* **2005**, *70*, 7558.

(3) Booker-Milburn, K. I.; Anson, C. E.; Clissold, C.; Costin, N. J.; Dainty, R. F.; Murray, M.; Patel, D.; Sharpe, A. *Eur. J. Org. Chem.* **2001**, 1473.

(4) Booker-Milburn, K. I.; Hirst, P.; Charmant, J. P. H.; Taylor, L. H. J. *Angew. Chem., Int. Ed.* **2003**, *42*, 1642.

(5) (a) Mazzocchi, P. H.; Bowen, M. J.; Narain, N. K. *J. Am. Chem. Soc.* **1977**, *99*, 7063. (b) Mazzocchi, P. H.; Minamikawa, S.; Bowen, M. J. *J. Org. Chem.* **1978**, *43*, 3079. (c) Mazzocchi, P. H.; Minamikawa, S.; Wilson, P. J. *J. Org. Chem.* **1979**, *44*, 1186. (d) Mazzocchi, P. H.; Wilson, P.; Khachik, F.; Klingler, L.; Minamikawa, S. *J. Org. Chem.* **1983**, *48*, 2981.

(6) For reviews of extensive studies on the PET chemistry of phthalimides, see: (a) Oelgemöller, M.; Griesbeck, A. G. In *CRC Handbook of Organic Photochemistry and Photobiology*, 2nd ed.; Horspool, W., Lenci, F., Eds.; CRC Press: Boca Raton, FL, 2004; Chapter 84, pp 1–19. (b) Yoon, U. C.; Mariano, P. S. In *CRC Handbook of Organic Photochemistry and Photobiology*, 2nd ed.; Horspool, W., Lenci, F., Eds.; CRC Press: Boca Raton, FL, 2004; Chapter 85, pp 1–15. (c) Yoon, U. C.; Mariano, P. S. In *Organic Photochemistry and Photophysics*; Ramamurthy, V., Schanze, K. S., Eds.; CRC Press: Boca Raton, FL, 2006; Vol. 14, Chapter 5, pp 179–206.

(7) Coyle, J. D. *Chem. Rev.* **1978**, *78*, 97.

(8) Maruyama, K.; Ishitoku, T.; Kubo, Y. *J. Org. Chem.* **1981**, *46*, 27.

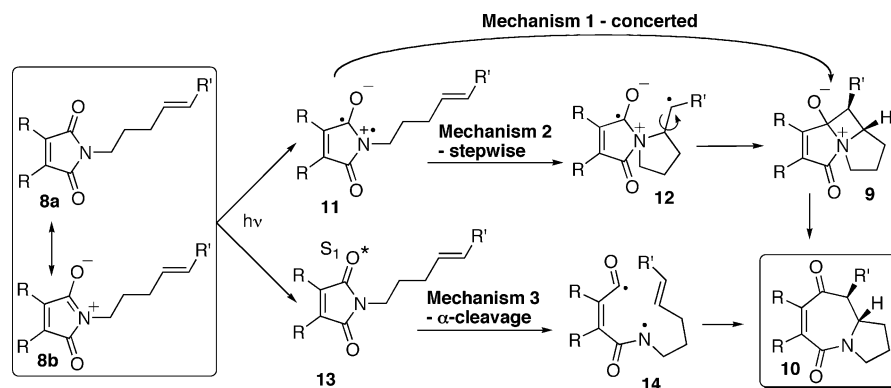
(9) Fischer, M. *Chem. Ber.* **1968**, *101*, 2669.

(10) Schutyser, J. A.; De Schryver, F. C. *Tetrahedron* **1976**, *32*, 251.

(11) Heerklotz, J. A.; Fu, C.; Linden, A.; Hesse, M. *Helv. Chim. Acta* **2000**, *83*, 1809.

(12) (a) Mazzocchi, P. H.; Thomas, J. J. *J. Am. Chem. Soc.* **1972**, *94*, 8281. (b) Mazzocchi, P. H.; Thomas, J. J. *J. Org. Chem.* **1979**, *44*, 50.

## SCHEME 2



Although we have observed retention of alkene geometry in the intramolecular cycloaddition reactions of a simple (*E*)-2-hexenyl-substituted maleimide, it is important to note that we have also observed loss of stereogenicity in other more complicated *Z*-substituted examples.<sup>13</sup> This could be a consequence of the maleimide acting as a sensitizer for an undesirable *Z* to *E* equilibration of the alkene or a fortuitous indication of a non-concerted pathway, implying that Mechanism 3 cannot be ruled out in our case. Furthermore, dichotomous behavior such as a competing intramolecular [2 + 2] cycloaddition within certain systems prompted us to undertake a detailed analysis of maleimide photochemistry using the modern laser and powerful calculation software packages available to us.

We have undertaken a detailed study of the wavelength-dependent kinetics and quantum yields of the [5 + 2] cycloaddition of substituted maleimides using the tunable laser facility. The study involved performing the [5 + 2] cycloaddition at several different wavelengths and measuring the relative rate of photoproduct formation and the quantum yield. It was reasoned that this study would enable the identification of the precise region of the UV spectrum where conversion to the [5 + 2] photoproduct was most efficient, thus pinpointing the key electronic transition involved. Such information would be

particularly important for dichloromaleimides, as our studies have shown that prolonged irradiation with broad-band Hg lamps results in significant photodecomposition in these substrates, seriously impacting overall yields and the utility of this reaction in total synthesis programs.

## Results and Discussion

The [5 + 2] cycloaddition of *N*-pentenyl dimethylmaleimide **4** to the azepine **5** was investigated over the wavelength range of 220–370 nm. This is generally a very efficient reaction that proceeds to completion in near-quantitative yields using a classic immersion well batch reactor in conjunction with high-powered medium-pressure UV Hg lamps. This system was chosen because the conversion to product is straightforward to follow accurately by NMR of the photosylate. Before any laser irradiations were attempted, a UV spectrum of **4** in acetonitrile was recorded over the wavelength range from 200 to 400 nm (see Figure 1 in Supporting Information).

The solution UV spectrum of **4** is dominated by a strong absorption maximum around 220 nm and a smaller feature at 265 nm which extends weakly to ~350 nm. As the formation of **5** was efficient under pyrex-filtered UV irradiation, it was initially assumed that the feature at 265 nm was the key transition responsible for the [5 + 2] photocycloaddition. It was expected that the rate of conversion and quantum yield would peak around this wavelength and decrease when experiments were conducted away from the  $\lambda_{\max}$  of this chromophore.

The first part of the study investigated how the quantum yield ( $\Phi$ ) of the [5 + 2] cycloaddition changed with wavelength over the 220–370 nm UV region spanning most of the absorption band(s) evident in Figure 1 (Supporting Information). For all wavelengths, it was decided to standardize quantum yield measurements at 3 min of irradiation ( $\Phi_{3\text{min}}$ ), as this time period allowed the formation of enough product to be accurately quantified by NMR.

The number of photons absorbed by the substrate was measured accurately from the power of the laser beam, the entirety of which was delivered to the sample. Corrections for any UV transmitted by the sample were made but were generally observed to be negligible for the shorter irradiation times. As expected, if the photochemical product also absorbed UV light, it was found that  $\Phi$  decreased over time, as can be seen for measurements made from a run at 330 nm. A plot of  $\Phi$  versus  $t$  at  $\lambda = 330$  nm shows that  $\Phi_{3\text{min}}$  is only slightly less (<0.02) than the extrapolated  $\Phi_{0\text{min}}$  value and can therefore be confidently used as an accurate absolute  $\Phi$  value for all subsequent

(13) Britton, H. C. Ph.D. Thesis, 2003, University of Bristol. As part of an attempted stemoamide synthesis, the photocycloaddition of various (*Z*)-alkenyl maleimides was studied and found to give variable results. For example, pure (*Z*)-**8a** (R = Me, R' = -CH<sub>2</sub>CH<sub>2</sub>OTBDMS) gave 78% of **10** (R = Me, R' = -CH<sub>2</sub>CH<sub>2</sub>OTBDMS) with a syn/anti ratio of 8.5:1. The analogous dichloromaleimides were more problematic; for example, pure (*Z*)-**8a** (R = Cl, R' = -CH<sub>2</sub>CH<sub>2</sub>OBn) gave **10** (R = Cl, R' = -CH<sub>2</sub>CH<sub>2</sub>-OBn) in 31% yield as a 1:1 mixture of the syn/anti isomers. The syn/anti isomers were separable via chromatography and appeared to be resistant toward equilibration.

(14) Frisch, M. J.; Trucks, G. W.; Schlegel, H. B.; Scuseria, G. E.; Robb, M. A.; Cheeseman, J. R.; Montgomery, J. A., Jr.; Vreven, T.; Kudin, K. N.; Burant, J. C.; Millam, J. M.; Iyengar, S. S.; Tomasi, J.; Barone, V.; Mennucci, B.; Cossi, M.; Scalmani, G.; Rega, N.; Petersson, G. A.; Nakatsuji, H.; Hada, M.; Ehara, M.; Toyota, K.; Fukuda, R.; Hasegawa, J.; Ishida, M.; Nakajima, T.; Honda, Y.; Kitao, O.; Nakai, H.; Klene, M.; Li, X.; Knox, J. E.; Hratchian, H. P.; Cross, J. B.; Bakken, V.; Adamo, C.; Jaramillo, J.; Gomperts, R.; Stratmann, R. E.; Yazyev, O.; Austin, A. J.; Cammi, R.; Pomelli, C.; Ochterski, J. W.; Ayala, P. Y.; Morokuma, K.; Voth, G. A.; Salvador, P.; Dannenberg, J. J.; Zakrzewski, V. G.; Dapprich, S.; Daniels, A. D.; Strain, M. C.; Farkas, O.; Malick, D. K.; Rabuck, A. D.; Raghavachari, K.; Foresman, J. B.; Ortiz, J. V.; Cui, Q.; Baboul, A. G.; Clifford, S.; Cioslowski, J.; Stefanov, B. B.; Liu, G.; Liashenko, A.; Piskorz, P.; Komaromi, I.; Martin, R. L.; Fox, D. J.; Keith, T.; Al-Laham, M. A.; Peng, C. Y.; Nanayakkara, A.; Challacombe, M.; Gill, P. M. W.; Johnson, B.; Chen, W.; Wong, M. W.; Gonzalez, C.; Pople, J. A. *Gaussian 03*, revision B.04; Gaussian, Inc.: Wallingford, CT, 2004.

(15) ter Steege, D. H. A.; Buma, W. J. *J. Chem. Phys.* **2003**, *118*, 10944.

(16) Climent, T.; Gonzalez-Luque, R.; Merchan, M. *J. Phys. Chem. A* **2003**, *107*, 6995.

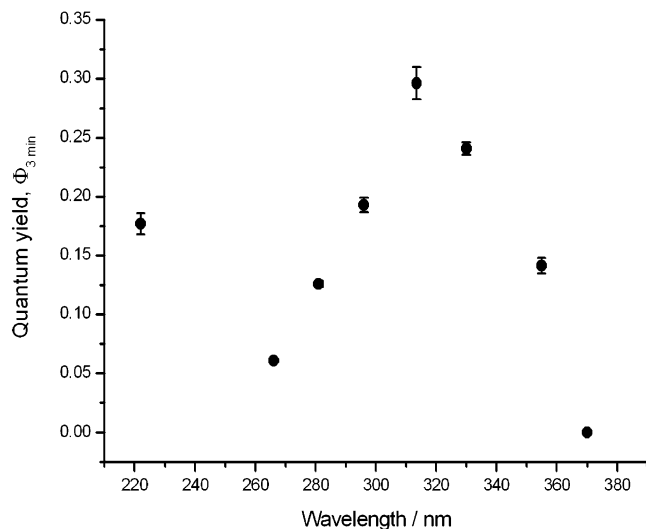


**FIGURE 3.** Plot of  $\Phi_{3\text{min}}$  versus wavelength for irradiations of **4**.

measurements over the various wavelengths of the study (see Figure 2 in Supporting Information).

Careful measurements of  $\Phi_{3\text{min}}$  versus  $\lambda$  for **4** over eight specific wavelengths from 222 to 355 nm were then obtained, and the data are presented in Figure 3. These data represent the first determination of absolute quantum yields for this class of cycloaddition at specific wavelengths, and values ranged from 0.0 to 0.3. From the plot, the key observation to note is that the quantum yield reaches a maximum at a wavelength of 313 nm ( $\Phi_{3\text{min}} = 0.3$ ), which is approximately 50 nm from the observed absorption maximum in the 250–300 nm region of the UV spectrum. Second,  $\Phi_{3\text{min}}$  decreased at wavelengths below 313 nm and actually reached a minimum at 266 nm, which is close to the  $\lambda_{\text{max}}$  of the first clear absorption band which we had initially taken to be the key excitation. It is interesting to note that, if the wavelength is decreased further to 222 nm,  $\Phi_{3\text{min}}$  actually increases again to 0.18. We suggest that the reason for this is internal conversion (IC) from a higher energy singlet state to the excited state responsible for the [5 + 2] cycloaddition.

To corroborate these intriguing results, investigations were undertaken of the rate of formation of photoproduct versus wavelength to look for correlations with the  $\Phi_{3\text{min}}$  data. At each excitation wavelength studied, data for irradiation-time-dependent conversion of the starting maleimide to photoproducts (measured from NMR spectra of the irradiated solutions) were observed to fit well to first-order kinetics over the first 15–20 min of exposure to 100 mW of laser power. Deviations from first-order kinetics are observed for irradiation times > 15 min (with some dependence on wavelength) and are most likely to be a consequence of the increasingly significant absorption by the product **5**. We thus report here phenomenological first-order rate constants for the irradiation of compound **4** with a constant 100 mW of UV power. The irradiation data from 266 nm are illustrative: from the fit to the data set, a phenomenological first-order rate constant for the [5 + 2] cycloaddition at 266 nm was obtained as  $k = 2.4 (\pm 0.15) \times 10^{-4} \text{ s}^{-1}$  (Figure 4). Under the conditions of our experiments and assuming no absorption of the UV laser radiation by the products of the photochemical reaction, zeroth-order kinetic behavior would be expected. The observed first-order kinetics can, however, be modeled by a scheme in which both the starting material and

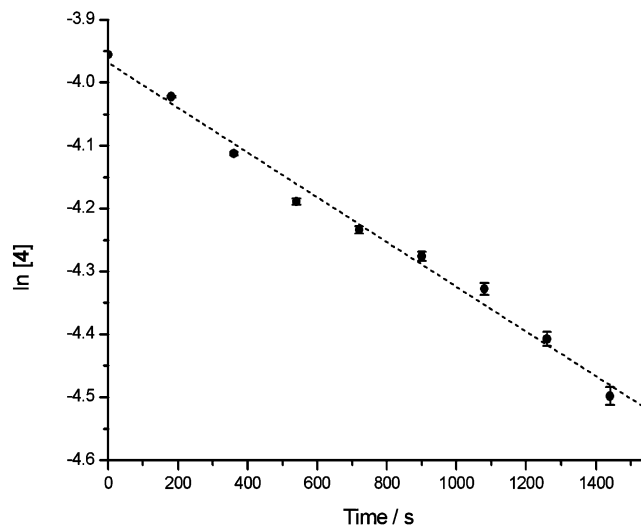


**FIGURE 4.** Representative plot of  $\ln[4]$  versus  $t$  for irradiation at 266 nm with 160 mW of power. Normalization of the gradient to 100 mW (standard for all subsequent measurements) gives the rate constant reported in the text.

the photoproduct absorb at the UV excitation wavelength (consistent with the decrease in  $\Phi$  versus  $t$ , as shown in Figure 2 in Supporting Information), with the assumption that the former can undergo cyclization to the latter but that the photoexcited state of the reaction product decays exclusively back to ground-state product molecules (by solvent-induced quenching). There is no evidence from NMR spectra of the irradiated samples that the UV absorption of the products induces any further chemical change. The first-order rate constants are reported with uncertainties that incorporate estimated errors in the measurements of concentrations from NMR spectra and the fit of time-dependent concentration data to a first-order kinetic model.

The same experiments were then conducted at all of the wavelengths used in the quantum yield study, and the derived phenomenological first-order rate constants were plotted as a function of wavelength. All experiments were conducted with an average laser power of 100 mW, and the results are shown in Figure 5. In the data analysis, rate constants were obtained from fits to data points for irradiation times from 0 to 900 s, as this was the region where data for all wavelengths best agreed with first-order kinetics. Deviations from linearity for plots of  $\ln[4]$  versus  $t$  for irradiation times of > 900 s are likely to arise from increasing absorption of laser photons by **5**, which became more significant at longer irradiation times.

The rate constant data are in excellent agreement with the  $\Phi$  data, in the sense that the peak in rate at  $\lambda = 313 \text{ nm}$  matches almost exactly the peak in  $\Phi$  for the cycloaddition. From these results, we conclude that the second strong absorption band in the UV spectrum of **4** (at  $\sim 265 \text{ nm}$ ) is not the primary absorption responsible for the [5 + 2] photocycloaddition. This 313–320 nm optimum wavelength for the cycloaddition is red shifted from the maximum of the dominant absorption and could correspond to the location of the actual  $\lambda_{\text{max}}$  of the chromophore responsible for the [5 + 2] cycloaddition. An additional electronic absorption primarily responsible for the reaction is not clearly evident as a separate feature in the UV spectrum because of overlapping bands and solvent broadening effects. Further analysis of the spectrum, as well as computational studies of



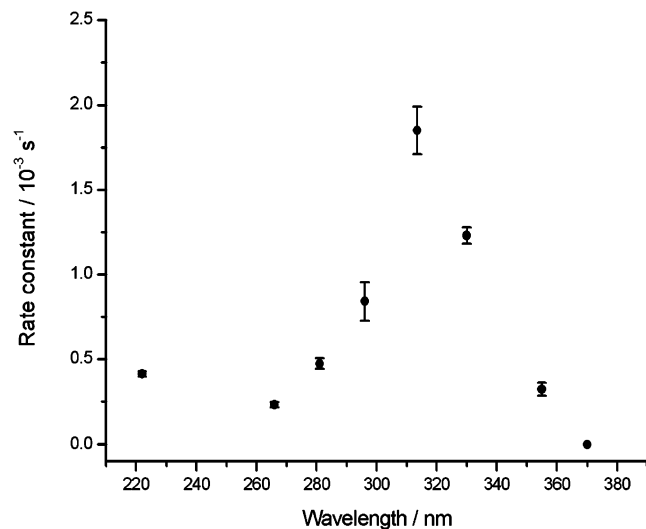


**FIGURE 5.** A plot of first-order photochemical rate constant  $k$  versus wavelength for irradiations of **4** at 222–370 nm.

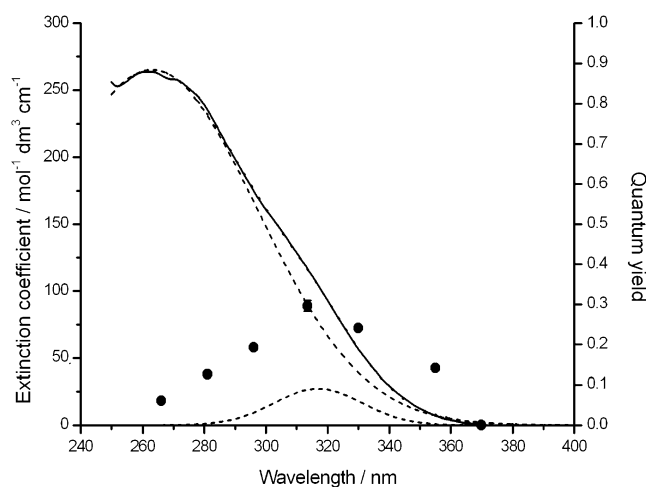


**FIGURE 6.** Deconvolution of the UV absorption spectrum of **4** in MeCN with quantum yield data overlaid for comparison. — Recorded UV spectrum; ----- deconvoluted spectra; ● quantum yield.

the electronic structure and energetics of low-lying excited states of representative maleimides, provides further insights.

To look for a possible further absorption feature in the UV spectrum of **4**, the absorption band spanning wavelengths from 250 to 350 nm was analyzed for evidence of more than one contribution.<sup>17</sup> A fit to two Gaussian line shapes with no constraints on width or position suggests there are indeed two overlapping features (Figure 6). There is a strong absorption band with a maximum at 263 nm and a smaller, red-shifted absorption band located with its maximum absorption at 318 nm.

This weak absorption band, implied by the deconvolution (and supported by rate and quantum yield data), is proposed to be the key transition responsible for the [5 + 2] cycloaddition of *N*-pentenyl dimethylmaleimide. In Figure 6, the variation in quantum yield of photocycloaddition is compared with the proposed deconvolution of the weak band peaking at 318 nm. The agreement in both width and shape of the  $\lambda$ -dependence of

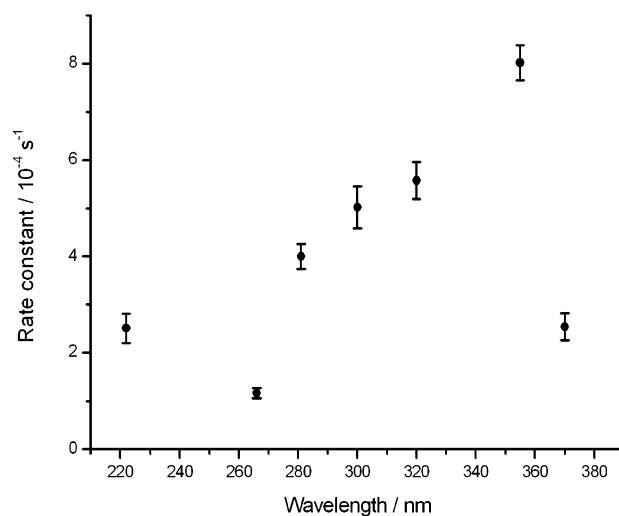
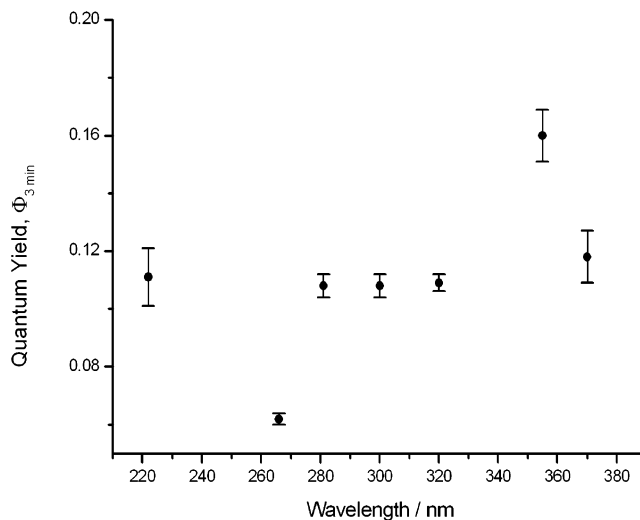


**FIGURE 8.** Measured values of (a)  $\Phi_{3\text{min}}$  and (b)  $k$  at different wavelengths for irradiations of **6**.

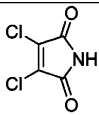
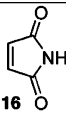
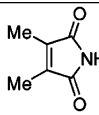
the two data sets is striking. Thus, the kinetic and quantum yield measurements appear to be selecting out the key absorption from within two or more overlapping electronic excitations with quite remarkable precision. It is clear that the [5 + 2] cycloaddition is a much more efficient reaction when the laser wavelength is tuned to the absorption maximum of this longer-wavelength feature.

As a further test of the arguments presented for the photoexcitation of **4**, a series of experiments were conducted on *N*-pentenyl-2,3-dichloromaleimide **6**, a substrate that also undergoes the [5 + 2] photocycloaddition to form a bicyclic azepine **7**. The UV spectrum of **6** shows similarities to the UV spectrum of **4** (see Figure 7 in Supporting Information).

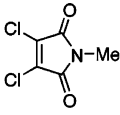
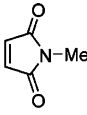
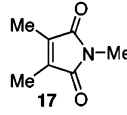
There is a strong, broad absorption from 200 to 260 nm and a weaker absorption with a maximum at approximately 310 nm. Chlorine substituents on the maleimide ring clearly red shift the observed absorptions. Measurements of  $\Phi_{3\text{min}}$  and  $k$  were conducted at the same wavelengths as those for substrate **4**. The plot of  $\Phi_{3\text{min}}$  versus  $\lambda$  (Figure 8a) shows that the cycloaddition of **6** is most efficient at 355 nm. Once again, this very precise laser approach demonstrates a significant deviation ( $\sim 50$  nm red shift) from the experimentally determined  $\lambda_{\text{max}}$  of  $\sim 310$  nm in the UV spectrum of **6**. While minima are observed

(17) For an example involving deconvolution of key features of bilirubin absorption spectra, see: Mazzoni, M.; Agati, A.; Troup, G. J.; Pratesi, R. *J. Opt. A: Pure Appl. Opt.* **2003**, *5*, S374.

**TABLE 1.** Gaseous Maleimide Excitation Assignments, Wavelengths, and Oscillator Strengths ( $f$ ) for the  $S_0 \rightarrow S_n$  Transitions with  $n = 1-4$  Calculated by TD-DFT at the B3LYP/6-31G(d,p) Level<sup>a</sup>

state									
	excitation	$\lambda / \text{nm}$	$f$	excitation	$\lambda / \text{nm}$	$f$	excitation	$\lambda / \text{nm}$	$f$
$S_0 \rightarrow S_1$	40 $\rightarrow$ 42 $^1B_1$ $n(O) \rightarrow \pi^*$	344.15	0.0002	25 $\rightarrow$ 26 $^1B_1$ $n(O) \rightarrow \pi^*$	368.95	0.0001	33 $\rightarrow$ 34 $^1A''$ $n(O) \rightarrow \pi^*$	348.36	0.0001
$S_0 \rightarrow S_2$	41 $\rightarrow$ 42 $^1B_2$ $\pi(N) \rightarrow \pi^*$	310.24	0.0367	23 $\rightarrow$ 26 $^1A_2$ $n(O) \rightarrow \pi^*$	300.27	0.0000	32 $\rightarrow$ 34 $^1A'$ $\pi(N) \rightarrow \pi^*$	288.30	0.0146
$S_0 \rightarrow S_3$	39 $\rightarrow$ 42 $^1A_2$ $n(O) \rightarrow \pi^*$	295.37	0.0000	24 $\rightarrow$ 26 $^1B_2$ $\pi(N) \rightarrow \pi^*$	274.00	0.0050	31 $\rightarrow$ 34 $^1A''$ $n(O) \rightarrow \pi^*$	287.03	0.0000
$S_0 \rightarrow S_4$	38 $\rightarrow$ 42 $^1B_2$ $\pi(C=C) \rightarrow \pi^*$	230.68	0.2561	22 $\rightarrow$ 26 $^1B_2$ $\pi(C=C) \rightarrow \pi^*$	214.35	0.2909	30 $\rightarrow$ 34 $^1A'$ $\pi(C=C) \rightarrow \pi^*$	216.49	0.3219

state									
	excitation	$\lambda / \text{nm}$	$f$	excitation	$\lambda / \text{nm}$	$f$	excitation	$\lambda / \text{nm}$	$f$
$S_0 \rightarrow S_1$	44 $\rightarrow$ 46 $^1A''$ $n(O) \rightarrow \pi^*$	341.19	0.0002	29 $\rightarrow$ 30 $^1A''$ $n(O) \rightarrow \pi^*$	364.79	0.0002	36 $\rightarrow$ 38 $^1A''$ $n(O) \rightarrow \pi^*$	344.48	0.0001
$S_0 \rightarrow S_2$	45 $\rightarrow$ 46 $^1A'$ $\pi(N) \rightarrow \pi^*$	330.10	0.0120	28 $\rightarrow$ 30 $^1A'$ $\pi(N) \rightarrow \pi^*$	305.04	0.0081	37 $\rightarrow$ 38 $^1A'$ $\pi(N) \rightarrow \pi^*$	311.19	0.0029
$S_0 \rightarrow S_3$	42 $\rightarrow$ 46 $^1A''$ $n(O) \rightarrow \pi^*$	296.77	0.0000	27 $\rightarrow$ 30 $^1A''$ $n(O) \rightarrow \pi^*$	301.51	0.0000	34 $\rightarrow$ 38 $^1A''$ $n(O) \rightarrow \pi^*$	288.07	0.0000
$S_0 \rightarrow S_4$	43 $\rightarrow$ 46 $^1A'$ $\pi(C=C) \rightarrow \pi^*$	241.24	0.2482	26 $\rightarrow$ 30 $^1A'$ $\pi(C=C) \rightarrow \pi^*$	216.07	0.2511	35 $\rightarrow$ 38 $^1A'$ $\pi(C=C) \rightarrow \pi^*$	221.94	0.3019

<sup>a</sup> The numbers in the excitation column denote the predominant orbitals involved in the transition and are followed by the symmetry label of the excited-state electronic configuration.

at 266 and 370 nm, the  $\Phi_{3\text{min}}$  actually increases again at 222 nm; as before, this is likely to be a result of excitation of a separate absorption band with subsequent internal conversion to the lower energy key excited state. The phenomenological first-order rate constant,  $k$  (at 100 mW average irradiation power), follows the same trend (Figure 8b). There is a peak in rate at 355 nm, and the minima in reaction rate occur at 266 and 370 nm. It is also evident that the [5 + 2] cycloaddition of **6** is a slower process than the [5 + 2] cycloaddition of **4** at the respective optimal wavelengths ( $k_4/k_6 = 2.34/1$ ). The above data further strengthen the argument that the [5 + 2] cycloaddition proceeds via excitation of a weak chromophore that is red shifted from the experimentally determined  $\lambda_{\text{max}} = \sim 310$  nm in the UV spectrum. Once again, this chromophore is likely to be the excitation responsible for the [5 + 2] photocycloaddition.

To progress further with interpretation of the experimental data, we sought additional information on the electronic absorption spectra of maleimides from accurate electronic structure theory calculations. Using TD-DFT, it was possible to compare the calculated energies of the electronic transitions with the suggested deconvolution of the absorption spectrum shown previously.

Table 1 shows the calculated wavelengths in the gas phase for transition to the first four electronically excited singlet states of six maleimides most relevant to this study. In particular, *N*-methyl-2,3-dimethylmaleimide **17** was chosen as the closest analogue of **4** that was appropriate for calculations at this level of theory. The excitation wavelengths are calculated from the energy gaps between the excited states and the electronic ground state, and the excitation energies correspond to vertical transitions that conserve the ground-state geometry. The calculated results for the parent maleimide **16** are in excellent agreement ( $\pm 5$  nm) both with the earlier calculations of ter Steege and Buma and with the key features reported in the gas-phase UV spectrum of **16**.<sup>18</sup> These calculations predict that there will be absorptions around 270–300 nm for the six maleimides, but there will also be absorptions at red-shifted wavelengths  $> 300$  nm corresponding to the  $S_0 \rightarrow S_1$  transition. The calculations indicate that the  $S_0 \rightarrow S_1$  transition is red shifted, on average, by 40–50 nm from the  $S_0 \rightarrow S_2/S_3$  transitions. This general

(18) For the gas-phase UV spectrum of maleimide, see: NIST WebBook. <http://webbook.nist.gov/cgi/cbook.cgi?ID=C541593&Units=SI&Mask=400#UV-Vis-Spec>.

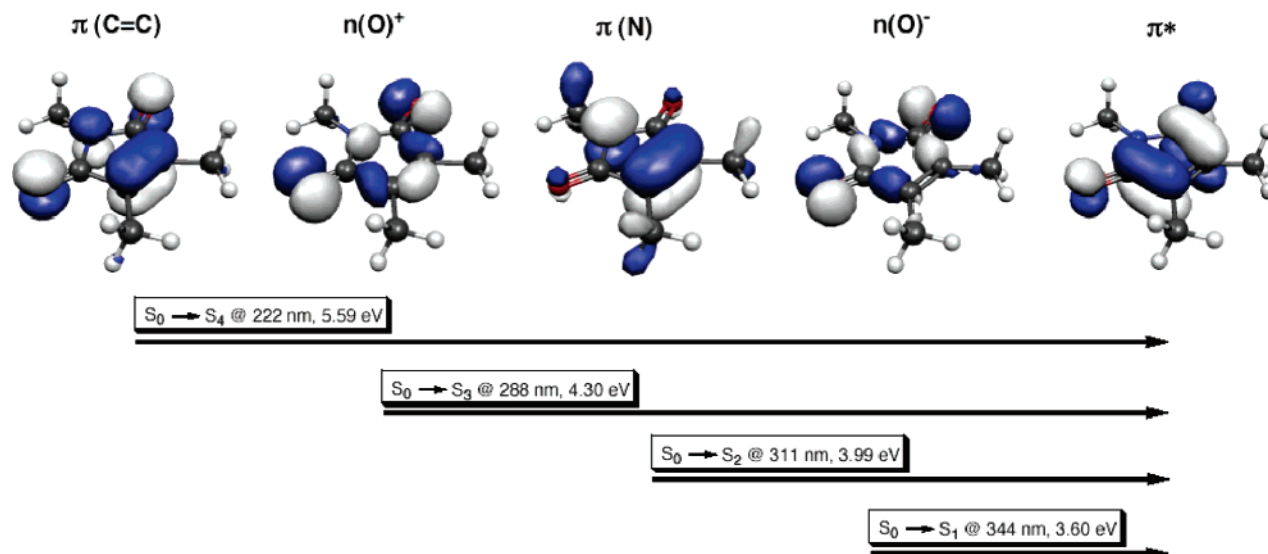


**FIGURE 9.** B3LYP-derived frontier molecular orbitals for **17**. The bottom part of the figure shows the single-electron orbital promotions, wavelengths, and energies for formation of the  $S_1$ ,  $S_2$ ,  $S_3$ , and  $S_4$  states.

trend in wavelength shift is in very good agreement with the separation of bands proposed for the deconvoluted UV spectrum of **4**. In particular, these calculated trends support the suggestion that the [5 + 2] cycloaddition of maleimides proceeds via excitation of a very weak absorption band red shifted from the experimentally determined  $\lambda_{\text{max}}$  at  $\sim 265$  nm that is not readily detected in the UV spectrum. The assignments presented in Table 1 for the molecular orbitals involved in the  $S_0 \rightarrow S_n$  transitions are based on interpretation of the results of the TD-DFT calculations and are consistent with the descriptions used by ter Steege and Buma for maleimide and *N*-methylmaleimide.<sup>15</sup> The frontier orbitals are plotted in Figure 9 for **17** and illustrate the choices of descriptions:  $n(\text{O})^-$  and  $n(\text{O})^+$  denote, respectively, orbitals that have a significant character of the antisymmetric and symmetric combinations of nonbonding O-atom orbitals;  $\pi(\text{N})$  and  $\pi(\text{C}=\text{C})$  denote  $\pi$  orbitals that extend around the five-membered ring but that have predominant N-atom  $p_z$ -orbital and  $\text{C}=\text{C}$   $\pi$ -orbital character.

For the parent maleimide **16**, a more detailed analysis of these data indicates that the  $S_0 \rightarrow S_1$  excitation at 368 nm is a result of an  $n(\text{O})^- \rightarrow \pi^*$  transition. The  $S_0 \rightarrow S_2$  excitation at 300 nm is predicted to be the  $n(\text{O})^+ \rightarrow \pi^*$  transition. Both of these have extremely weak calculated oscillator strengths and maximum extinction coefficients which are entirely consistent with this classically forbidden carbonyl transition ( $f = 0.0001$ ; calculated  $\epsilon_{\text{max}} \approx 10 \text{ mol}^{-1} \text{ dm}^3 \text{ cm}^{-1}$ , in excellent agreement with the experimental value for the  $\sim 350$  nm band). The third main feature,  $S_0 \rightarrow S_3$ , at 274 nm is an interesting excitation resulting from a predicted  $\pi(\text{N}) \rightarrow \pi^*$  transition from a hybrid molecular orbital localized over the maleimide nitrogen and  $\text{C}=\text{C}$  centers and is predicted to be much stronger than the  $n \rightarrow \pi^*$  transitions ( $f = 0.005$ ; calculated  $\epsilon_{\text{max}} \approx 200 \text{ mol}^{-1} \text{ dm}^3 \text{ cm}^{-1}$ , consistent with the experimental value for the band centered around 270 nm).  $S_0 \rightarrow S_4$  is predicted to be the  $\pi \rightarrow \pi^*$  transition of the conjugated maleimide  $\text{C}=\text{C}$  bond and has a high calculated oscillator strength ( $f = 0.2909$ , calculated  $\epsilon_{\text{max}} \approx 7500 \text{ mol}^{-1} \text{ dm}^3 \text{ cm}^{-1}$ ), consistent with this type of transition, and correlates very closely with the prominent feature in the 200–250 nm region of the measured gaseous<sup>18</sup> and solution UV spectra (with  $\epsilon$  values of up to  $10\,000 \text{ mol}^{-1} \text{ dm}^3 \text{ cm}^{-1}$ ).

For *N*-methyl-2,3-dimethylmaleimide **17**, the closest analogue to **4**, the ordering of the transitions now changes;  $S_0 \rightarrow S_2$  is now a  $\pi(\text{N}) \rightarrow \pi^*$  transition that is red shifted to 311 nm. The two carbonyl transitions are now blue shifted with  $n(\text{O})^- \rightarrow \pi^*$  ( $S_0 \rightarrow S_1$ ), calculated to lie at 344 nm. Solvent correction for **17** gives approximate values for the transitions  $S_0 \rightarrow S_1$  at 335 nm and  $S_0 \rightarrow S_2$  at 322 nm, which are in good agreement with the laser-determined kinetic/quantum yield data and the very weak feature ( $\sim 320$  nm) from the deconvoluted spectrum for **17**. The frontier molecular orbitals for all of the transitions involved in **17** are depicted in Figure 9.

**Mechanistic Implications.** In order to use this detailed information as part of a mechanistic analysis, it is first necessary to ascertain which orbitals are those most likely involved in the [5 + 2] photocycloaddition of **4** and **6**. For **17**, both  $S_0 \rightarrow S_1$  and  $S_0 \rightarrow S_2$  transitions are predicted to be very similar in energy and to occur at wavelengths very close to the optimum value determined by the laser experiments ( $\sim 320$  nm). Since  $S_0 \rightarrow S_2$  is a  $\pi(\text{N}) \rightarrow \pi^*$  transition, it would be expected to be a considerably stronger feature in the UV spectrum than the symmetry forbidden  $n \rightarrow \pi^*$  excitation predicted for  $S_0 \rightarrow S_1$ . This is born out by comparing the oscillator strengths of **17** to the measured and deconvoluted spectra for **4**; that is, the feature identified at  $\sim 320$  nm would appear to be far too weak for a  $\pi(\text{N}) \rightarrow \pi^*$  transition with  $f = 0.0029$ . Extinction coefficients at the maxima of the UV absorption bands, estimated from the computed oscillator strengths for the  $\pi(\text{N}) \rightarrow \pi^*$  and  $n(\text{O})^- \rightarrow \pi^*$  transitions ( $47$  and  $7 \text{ mol}^{-1} \text{ dm}^3 \text{ cm}^{-1}$ , respectively, assuming band fwhm's of 90 and 30 nm based on the experimental spectrum), are consistent with experimental values derived from the deconvoluted bands shown in Figure 6 ( $265$  and  $28 \text{ mol}^{-1} \text{ dm}^3 \text{ cm}^{-1}$  for the  $\sim 260$  and  $\sim 320$  nm bands, respectively). This information, coupled with the fact that the calculations indicate that the  $S_0 \rightarrow S_1$  transition is always  $n(\text{O})^- \rightarrow \pi^*$  for all six maleimides and consistently red shifted from the  $\pi(\text{N})$ ,  $n(\text{O})^+ \rightarrow \pi^*$  transitions, leads us to propose that the key excitation for maleimide [5 + 2] cycloaddition chemistry is the  $n(\text{O})^- \rightarrow \pi^*$  transition indicated in Figure 9.

This information can be used to make several comments regarding the likely mechanism of maleimide [5 + 2] photo-

cycloaddition. (a) We believe that it is unlikely that the concerted Mechanism 1 (Scheme 2) operates because the TD–DFT results indicate that the nitrogen lone pair is not involved in the initial  $S_0 \rightarrow S_1$  transition. It is important to note that none of the DFT-generated molecular orbitals indicate that there is any significant contribution from a resonance canonical form relating to **8b**. It is difficult to see how a concerted cycloaddition could proceed in the absence of any significant  $\pi$  density in the imide C–N bond in question. (b) Excitation of an electron from the  $\pi(N)$  molecular orbital to  $\pi^*$  ( $S_0 \rightarrow S_2$ , Figure 9) could lead to a species with radical-cation character on nitrogen (cf. **11**, Scheme 2) and thus partially argue in favor of Mechanism 2. However, the same arguments put forward in (a), coupled with the predicted strength of this absorption ( $f = 0.0029$ ), make a relatively strong case against this mechanism. (c) The calculated and measured data are supportive of proposed Mechanism 3 whereby the  $S_1$  state **13** undergoes a classic  $\alpha$ -cleavage followed by a rapid cyclization sequence. Examination of the MOs demonstrates that, nominally, the  $n(O)^- \rightarrow \pi^*$  excitation reduces the  $\sigma$ -bonding character of the requisite C–N bond and thus may encourage the  $\alpha$ -cleavage. Of course, in this sequence, ring closure of **14** would need to be faster than any bond rotations to preserve initial alkene stereochemistry where this is observed. Conversely, bond rotation in this pathway would also account for examples where we have observed loss of stereogenicity. (d) It must be stressed, however, that these interpretations do not take into account alternative fates for the likely  $S_1$  state **13**. For example, it is possible that singlet species such as **11** are derived from **13** by internal conversion between the  $S_1$  and  $S_2$  states; the TD–DFT calculations suggest there is very little energy difference between these. If such a process were responsible for the cyclization, however, it is reasonable to suppose that direct excitation of the  $S_2$  state would promote the conversion, but this is contrary to the experimental observations. (e) We have also considered carefully the possibility of two-photon processes and discount these for a number of reasons. The one-photon  $n(O)^- \rightarrow \pi^*$  absorption step is formally symmetry forbidden and thus weak; therefore, the transient density of excited-state molecules is likely to be low, making subsequent photon absorption of low probability during the laser pulse. The laser pulse duration is  $\sim 10$  ns, but the interval between pulses is 50 ms; therefore, any multiphoton absorption would have to occur within a single laser pulse. The rate of the second photon absorption must compete with the timescales for intramolecular reaction and solvent quenching, both of which are likely to be fast, subnanosecond processes. The  $S_1$  excited state may also undergo conventional ISC to a longer-lived  $T_1$  state that does not undergo cycloaddition but which might exist long enough to be exposed to multiple laser pulses. It is then conceivable that this longer-lived state undergoes further excitation to **11** because of the likely density of excited triplet states in the vicinity of the two-photon energy. The solutions undergoing irradiation are, however, rapidly stirred so that buildup of  $T_1$ -state molecules in the small volume of the UV laser beam will not occur. ISC, absorption of the second photon, and subsequent reaction from a  $T_n$  state would have to happen with very high efficiency to account for the observed quantum yields of products.

## Summary

Wavelength-tunable, pulsed UV lasers have been used to investigate the wavelength dependence of the  $[5 + 2]$  photo-

cycloaddition of *N*-pentenyl-3,4-disubstituted maleimides. First values of the quantum yield and phenomenological rate constants for these reactions have been measured over a series of wavelengths. The results show that the quantum yield and rate are not greatest at the measured absorption maximum in the 260–310 nm region of the UV spectrum. The maxima in rate and quantum yield for dimethylmaleimide **4** have been experimentally determined to occur at approximately 320 nm, substantially red shifted from the observed absorption maximum. The corresponding dichloromaleimide **6** shows the same trends, with quantum yields and rates that peak at a wavelength red shifted some 50 nm from the measured  $\lambda_{\max}$ . Analysis of the UV spectrum and complementary electronic structure theory calculations by TD–DFT methods of six simpler model maleimides indicate the presence of a weak absorption at longer wavelength with a  $\lambda_{\max}$  that correlates well with the observed maxima in quantum yield and rate constant. These studies conclude that the key  $S_0 \rightarrow S_1$  transition is  $n \rightarrow \pi^*$  in nature and that a fragmentation/cyclization mechanism can be rationally implicated to account for this.

Overall, this study demonstrates that modern, tunable UV lasers are precision tools for identifying the key electronic transitions often buried in the continuum of even the most high-resolution UV spectra of organic molecules. Once obtained, these results can be coupled with high-level electronic structure calculations, thus providing opportunities to rationalize the complex mechanisms of this class of photochemical reactions as well as the ability to optimize these for scale-up.

## Experimental Procedures

**Laser UV Generation.** Wavelengths from 280 to 370 nm. The 532 nm (second harmonic) output of a frequency-doubled  $Nd^{3+}$ :YAG laser operating at a 20 Hz repetition rate was used to pump a dye laser containing one of the following laser dyes: Rhodamine 6G, Rhodamine B, DCM, Styryl 8. The generated visible radiation of precise wavelength was frequency doubled in a KDP (potassium dihydrogen phosphate) crystal and separated from undoubled laser radiation by a Pellin–Broca prism. The resulting UV output was typically 5–9 mJ/pulse, giving UV powers in the range of 100–180 mW.

The 355 nm wavelength was obtained using a third-harmonic generation crystal (KDP) to combine the fundamental (1064 nm) and second harmonic (532 nm) wavelengths of the  $Nd^{3+}$ :YAG laser operating at a 20 Hz repetition rate. Typical pulse energies were selected to be 6 mJ/pulse (120 mW).

The 266 nm wavelength was obtained using a fourth-harmonic generation crystal (KDP) to double the frequency of the second harmonic (532 nm) of the  $Nd^{3+}$ :YAG laser operating at a 20 Hz repetition rate. Typical pulse energies were selected to be 8 mJ/pulse (160 mW).

The 222 nm wavelength was obtained using the dual 355 and 532 nm outputs of a  $Nd^{3+}$ :YAG laser operating at a 30 Hz repetition rate. The 532 nm radiation was used to pump a dye laser containing Rhodamine B dye. The 596 nm radiation generated from the dye laser was then mixed with the 355 nm output in a BBO crystal to produce 222 nm UV radiation. Pulse energies were typically 3 mJ/pulse (90 mW).

All laser powers were measured immediately before and after irradiation of samples using a Molectron 500A power meter. Any UV transmitted by the irradiated samples was continually monitored during measurement of photochemical quantum yields.

**Sample Irradiations.** The *N*-pentenyl maleimides **4** and **6** were prepared by Mitsunobu coupling of the respective maleimides and 4-pentene-1-ol as described previously.<sup>3</sup> UV/visible spectra of the photochemical precursors were performed on a UV/visible spec-



trophotometer in a 1 cm far-UV quartz cuvette. A 0.02 M batch solution of **4** and a 0.014 M batch solution of **6** in acetonitrile were prepared and degassed with nitrogen. For kinetic measurements, a 3 mL aliquot of the maleimide solution was placed inside a far-UV quartz cuvette equipped with a PTFE magnetic stir bar. The cuvette was then irradiated at a particular wavelength while stirring, ensuring that the laser beam entered the center of the cuvette at least 5 mm above the stirring bar. After the appropriate time period, the cuvette was removed, and a freshly filled cuvette was placed in front of the beam for the next appropriate time period. Each subsequent cuvette was irradiated for 3 min longer than the previous one, starting from  $t = 3$  min up to  $t = 25$  min. For quantum yield ( $\Phi$ ) measurements, the  $t = 3$  min cuvette was used at each wavelength. Once all of the irradiations had been completed, the laser system was adjusted to perform irradiations at a different wavelength, and the procedure was repeated. Conversion of the starting material to the [5 + 2] photoproduct was monitored by evaporation of each cuvette in vacuo, and the entire contents redissolved in  $\text{CDCl}_3$  and was analyzed by 400 MHz  $^1\text{H}$  NMR spectroscopy. Comparison of the integrals of the vinyl protons in **4/6** with the  $\alpha$ -keto methylene protons in **5/7** gave accurate maleimide versus cycloadduct ratios for the reliable measurement of  $\Phi$  (at low conversion) over the variety of wavelengths quoted.

**Computational Section.** The many resonance forms that can be drawn for photoexcited maleimides suggest an extensive delocalization of electron density in the ground and excited states. To aid understanding of the electronic character of the excited states, vertical excitation energies of the low-lying singlet and triplet electronic states of representative maleimide-based molecules were carried out with time-dependent density functional theory (TD-DFT) using the Gaussian 03 suite of programs.<sup>14</sup> The TD-DFT calculations were performed using the hybrid B3LYP functional in conjunction with the 6-31G(d,p) split-valence basis set, which were also used to obtain optimized geometries and conduct harmonic vibrational frequency analysis. The TD-DFT results provide the symmetries of the electronically excited states and identify the dominant electronic promotions giving rise to them. Although several of the possible excitations from the ground state

to higher-lying singlet states are electronically forbidden by one-photon electric dipole selection rules, they can become allowed through vibrational–electronic (vibronic) coupling of vibrational modes that are not totally symmetric. In addition to calculations for isolated gas-phase molecules, the effects of solvation by acetonitrile were incorporated using the polarizable continuum model (PCM) to examine their influence on the ordering of the electronically excited states. To simplify the computational studies, calculations were carried out for smaller model systems. Maleimide, its substituted variants 2,3-dimethylmaleimide and 2,3-dichloromaleimide, and their N-methylated analogues were chosen as model systems to examine the effects of substitution at the carbon and nitrogen sites. Outcomes of calculations on maleimide are in good accord with previous DFT and TD-DFT calculations by ter Steege and Buma,<sup>15</sup> but they show discrepancies with the results of MS-CASPT2 calculations of the valence states by Climent et al.<sup>16</sup> Reasons for these discrepancies were not explored in detail, but test CASPT2 calculations with a 6-311G\* basis set and a 12-electron and 9-orbital active space gave excited-state energies in good agreement (to within 0.12 eV for the first three excited singlet states and the first triplet state) with our TD-DFT calculations.

**Acknowledgment.** We thank EPSRC (GR/S25593) and GSK for generous funding, Roger Alder and Jeremy Harvey for invaluable guidance on the calculations and stimulating discussion and advice on mechanistic implications, and Keith N. Rosser for help with the lasers. A.J.O.E. thanks the Leverhulme Trust for the award of a Senior Research Fellowship.

**Supporting Information Available:** Tables of laser data for quantum yield and rate determination; TD-DFT-calculated singlet and triplet energies, wavelengths, and oscillator strengths for maleimides; Figures 1, 2, and 7 showing UV absorption spectra and quantum yield measurements. This material is available free of charge via the Internet at <http://pubs.acs.org>.

JO062316G